Microwave enhanced ion-cut silicon layer transfer

D. C. Thompson, T. L. Alford, J. W. Mayer, T. Höchbauer, J. K. Lee, M. Nastasi, S. S. Lau, N. David Theodore, and Paul K. Chu

Citation: Journal of Applied Physics **101**, 114915 (2007); doi: 10.1063/1.2737387
View online: http://dx.doi.org/10.1063/1.2737387
View Table of Contents: http://scitation.aip.org/content/aip/journal/jap/101/11?ver=pdfcov
Published by the AIP Publishing

Microwave enhanced ion-cut silicon layer transfer

D. C. Thompson, T. L. Alford,[a] and J. W. Mayer
School of Materials, Arizona State University, Tempe, Arizona 85287

T. Höchbauer, J. K. Lee, and M. Nastasi
Materials Science and Technology Division, Los Alamos National Laboratory, Los Alamos, New Mexico 87544

S. S. Lau
Department of Electrical and Computer Engineering, University of California at San Diego, San Diego, California 92093

N. David Theodore
Wireless and Packaging Systems Laboratory, Freescale Semiconductor Incorporated, Tempe, Arizona 85284

Paul K. Chu
Department of Physics and Materials Science, City University of Hong Kong, Tat Chee Avenue, Kowloon, Hong Kong

(Received 13 February 2007; accepted 30 March 2007; published online 13 June 2007)

Microwave heating has been used to decrease the time required for exfoliation of thin single-crystalline silicon layers onto insulator substrates using ion-cut processing. Samples exfoliated in a 2.45 GHz, 1300 W cavity applicator microwave system saw a decrease in incubation times as compared to conventional anneal processes. Rutherford backscattering spectrometry, cross sectional scanning electron microscopy, cross sectional transmission electron microscopy, and selective aperture electron diffraction were used to determine the transferred layer thickness and crystalline quality. The surface quality was determined by atomic force microscopy. Hall measurements were used to determine electrical properties as a function of radiation repair anneal times. Results of physical and electrical characterizations demonstrate that the end products of microwave enhanced ion-cut processing do not appreciably differ from those using more traditional means of exfoliation. © *2007 American Institute of Physics*. [DOI: 10.1063/1.2737387]

INTRODUCTION

Ion-beam modification of materials, combined with engineering of materials properties, has given life to silicon on insulator (SOI) and silicon on heterogeneous layered device technologies. The process of exfoliating a thin layer of silicon by ion implantation of selected species and bonding to a suitable substrate followed by exfoliation, termed "ion cutting," has improved dramatically since its invention[1,2] due to continued research in the effects of process parameters on materials properties. Ion-cut fabrication is a desirable alternative in SOI technology because the end product is a layer of single crystal silicon, which leads to more desirable electrical characteristics such as increased carrier mobility, carrier lifetimes, and switching frequencies. Ion-cut fabrication process parameters such as implant species, dose, beam energy, temperature, and lattice strain have all had profound effects on the ion-cut process. As a result, what started as research into lessening the effects of hydrogen in silicon has now blossomed into finding ways to enhance those same effects.[3,4]

Since the discovery that silicon layer transfer by ion implantation is critically influenced by ion implant dose, beam energy, and annealing at high temperatures, ion-cut research has focused on tailoring those parameters in order to process ion-cut fabricated samples faster, cheaper, and with reduced implant-induced damage. Researchers have pursued minimizing implant-induced damage because damage due to the ion-implant step of fabrication serves to partially nullify the benefits of the process. For the beam energies and doses needed in ion-cut fabrication the implant-induced damage results in a thin layer of amorphous silicon. Amorphous layers of silicon are common in other SOI process methods, but undesirable in ion-cut processing because amorphous silicon results in electrical properties that are less desirable than those of single crystal silicon.[5]

In order to maximize the desirable effects of the ion-cut process, research on ion-cut mechanisms began shortly after discovery. Researchers found that the same implant-induced damage which can lead to difficulties in desired electrical behavior is actually integral to the ion-cut process.[6–8] To improve electrical characteristics, implant damage could then be removed with repair anneals, selective etching, or flash polishes.[9] Investigation into the use of boron demonstrated a decrease in damage associated with the hydrogen implant, at the cost of high doses of boron.[10] More recent work has centered on alternative methods to ion implantation which result in the same product, without large amounts of implant-induced damage.[11] The central theme in such investigations is that implant-induced lattice damage is undesirable, and unless polishing or etch techniques are used, mostly unavoidable.

This work centers on an alternative approach to dealing with the ion implant-induced damage associated with ion-cut

[a]Electronic mail: alford@asu.edu

fabrication. In this work the authors researched a process technique which, by the nature of the physics involved, served to enhance the ion-cut processing by the inclusion of ion implant damage. This research involves microwave frequency heating to initiate the exfoliation process in ion-cut fabrication. Microwaves have been of increased interest for both steady state and rapid thermal anneal processing due to desirable side effects. Microwave heating has become a viable alternative for thermal synthesis, sintering, and joining of ceramic materials.[12–14] In silicon, microwaves have been used to activate solid state reactions.[15,16]

The attractive nature of microwave heating lies in the volumetric heating that microwaves enable. With volumetric heating with microwaves the power input needed for a given temperature rise is less than other rapid thermal processing.[17] In ion-cut fabricated samples the region of interest is within the penetration depth of most microwave processing equipment. Therefore less power is demanded in microwave heating of ion-cut samples than other techniques. This effect attracted the authors to study the effects of microwave heating of ion-cut fabricated materials.

EXPERIMENT

To fabricate the samples used in this work Czochralski (CZ) grown, *p*-type boron doped, 1–13 Ω cm (100) orientated silicon wafer pieces were cleaned using a Radio Corporation of America (RCA) procedure. The cleaned silicon was placed in a Varion/Extrion Division 200-DF4 ion implanter. Samples used for blistering experiments were implanted with $(0–1)\times10^{15}$ cm^{-2}, 147 keV B^+ ions and $(4–6)\times10^{16}$ cm^{-2}, 40 keV H^+ ions at liquid nitrogen temperatures. Samples used for layer transfer experiments were implanted with $(0–3)\times10^{15}$ cm^{-2}, 175 keV B^+ ions and $(4.5–5)\times10^{16}$ cm^{-2}, 100 keV H_2^+ ions at room temperature. Because the H_2^+ ions fragment at the surface, this implant process is equal to the implantation of atomic hydrogen at 50 keV and a dose of $9\times10^{16}–1\times10^{17}$ cm^{-2}. Samples to be used to realize blistering in microwaves were placed in a 2.45 GHz, cavity applicator microwave system where they were processed for time durations of up to 30 min using 1300 W microwaves. Temperature profiles on the sample surfaces were monitored using a Raytek Compact MID series pyrometer.

For samples being used in coherent layer transfer, separate nonimplanted silicon pieces were coated with a chemically grown oxide to a thickness of approximately 500 nm. Both the implanted silicon and the nonimplanted silicon with oxide layer were then RCA cleaned and placed in a Tegal asher at 100 °C for plasma surface activation using a 300 W, 13.56 MHz, 140 cm^3 min^{-1} oxygen rf plasma. After plasma activation, de-ionized water rinsing, and spin drying, the wafers were placed in surface-to-surface direct contact at room temperature. The bonded pairs were subsequently annealed in a mechanical furnace at 100 °C for 2 h to drive out any residual water at the bond interface. After mechanical furnace annealing, the implanted and bonded silicon samples were placed in a 2.45 GHz, 1300 W cavity applicator microwave system where they were processed for time durations ranging from 12 to 180 s before layer transfer was visually observed. Temperature profiles on the sample surfaces were monitored using a Raytek Compact MID series pyrometer. Figure 1 depicts the implant, surface activation, bonding, and annealing steps used in the microwave cut fabrication process.

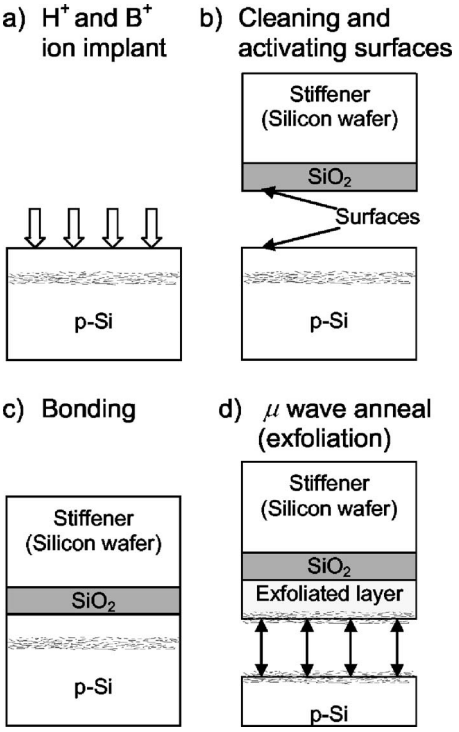

FIG. 1. Schematic of the microwave enhanced ion-cut process: (a) boron and/or hydrogen implant, (b) cleaning and surface activation, (c) bonding, and (d) microwave exfoliation.

Samples were physically and electrically characterized after exfoliation. Samples not bonded to a stiffener were physically characterized using optical and scanning electron microscopy (SEM). For optical imaging, a Zeiss Axiophot microscope was employed. A HITACHI S-4700 SEM, equipped with field emission gun and operating at a terminal voltage of 15 kV, was used to examine blistered surface morphology and blister depth.

The as-transferred SOI surface quality was physically characterized using a Nanoscope IIIE atomic force microscope (AFM) in tapping mode in order to determine the root mean square (rms) surface roughness of the transferred layers. To determine transferred layer thickness and crystalline quality samples were analyzed using Rutherford backscattering spectrometry (RBS) with a 2.0 MeV He^{++} analyzing beam. The detector was positioned 13° from the incident beam. RUMP[18] software was used to simulate layer thickness from RBS data. To examine crystalline quality and determine transferred layer thicknesses cross sectional transmission electron microscopy (XTEM) was employed using a Philips CM200-FEG TEM operating at a voltage of 200 kV. To electrically characterize transferred layers, Hall effect measurements were obtained using an EKG HEM 2000 in order to quantify transferred layer resistivity, mobility, carrier type, and carrier concentration.

To evaluate the effects of microwave annealing on the

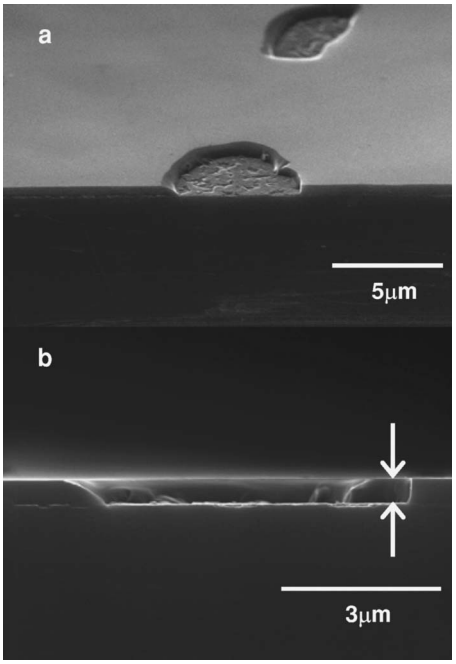

FIG. 2. Scanning electron micrograph of an exfoliated surface (a) at approximately 45° to the surface normal and (b) in cross section. The sample pictured was implanted with 6×10^{16} H^+ cm^{-2}.

electrical characteristics of transferred layers after radiation repair, samples were annealed in a vacuum carousel furnace with temperatures ranging from 500 to 800 °C, for time durations between 2 and 4 h, at a pressure of 10^{-7} Torr. The anneals were followed by more electrical measurements, TEM, and RBS in order to characterize the repair of any radiation damage that may have been created in the ion-cut process.

RESULTS

Ion implanted samples were first microwave annealed without bonding to substrates in order to provide proof of concept for using microwaves as a viable alternative to traditional annealing in the ion-cut process. Optical imaging determined if exfoliation of implanted samples occurred. Blistering occurred in samples with hydrogen concentrations greater than 4×10^{16} H^+ cm^{-2}. Using optical means exfoliated blister depths could not be determined to a reasonable level of certainty. Exfoliated surfaces were therefore examined using a SEM in cross section (XSEM).

Figure 2 depicts an exfoliated surface, cleaved to allow examination using a SEM in cross section. XSEM has proven to be a viable technique for estimating ion-cut depths for transferred layers without fabricating bonded samples.[6,10] To examine an exfoliated blister in cross section the authors cleaved a sample along a major crystallographic plane in a highly exfoliated area and then examined the cleaved interface for blistered areas in cross section. Part (a) of Fig. 2 highlights the exfoliated and cleaved surfaces while part (b) demonstrates the cross section of the exfoliated surface in part (a). Using XSEM figures such as Fig. 2(b), the average blistered surface depth in samples measured using XSEM was approximately 410 nm.

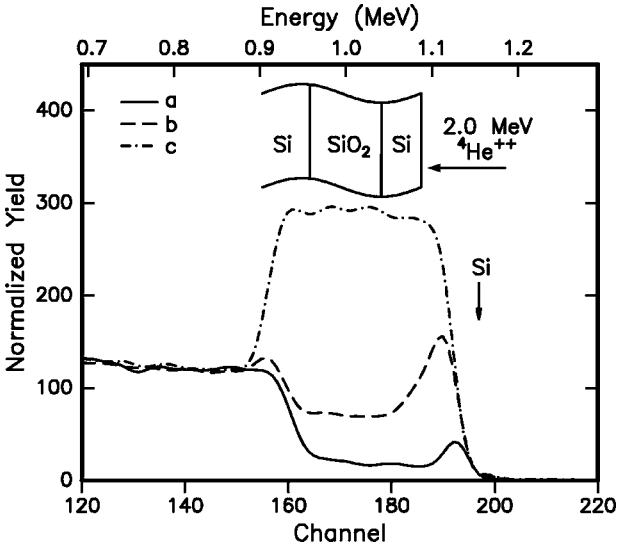

FIG. 3. RBS spectra from a thin layer of exfoliated silicon on insulator (a) [001] channeled orientation after radiation repair, (b) [001] channeled orientation "as cut," and (c) random orientation as cut.

Figure 3 presents an example of the RBS spectra obtained from samples fabricated using steps (a)–(d) outlined in the ion-cut process of Fig. 1. The RBS spectra shown in Fig. 3 include both random and [001] channeled orientations of SOI samples. Spectra from both random and channeled orientations demonstrate that the ion-cut process was successful in using microwaves to initiate the exfoliation, and coherent layer transfer, of single crystal silicon.[19,20] Spectrum (c), obtained from an "as-cut" sample in random orientation, indicates the presence of a continuous layer of silicon on top of the insulator, while also hinting at a mild surface microroughness as is evident from the width of the low energy edge at channels 150–160.[20] RUMP simulation of the RBS spectra (c) determined the thickness of the transferred layer to be 475 nm and that of the oxide layer 500 nm. Spectrum (b), obtained from a [001] aligned sample of as-cut SOI, shows a dramatic decrease in yield, indicating that the transferred layers have kept most their crystallinity. The width of the surface peak in the as-cut channeled spectrum (b) indicates that the majority of the radiation damage was concentrated at the top of the transferred layer. When comparing channeled spectrum (a), obtained from an annealed transferred layer, and channeled spectrum (b), obtained from the as-cut transferred layer, the spectra indicate that most of the radiation damage was repaired upon further annealing of the microwave initiated ion-cut samples. When viewing the RUMP simulations of RBS spectra for the entire population of cut samples involving the transfer of a coherent layer, the transferred layer thicknesses ranged between 475 and 500 nm. These findings compare well with previous ion-cut techniques.[21–23]

Figure 4 displays electron diffraction patterns and XTEM images of a typical microwave cut sample. The images displayed in Fig. 4(a) demonstrate the as-cut transferred layer quality, while Fig. 4(b) displays the quality of the microwave cut sample after several successive high temperature anneals. The anneals range 500–800 °C and were done

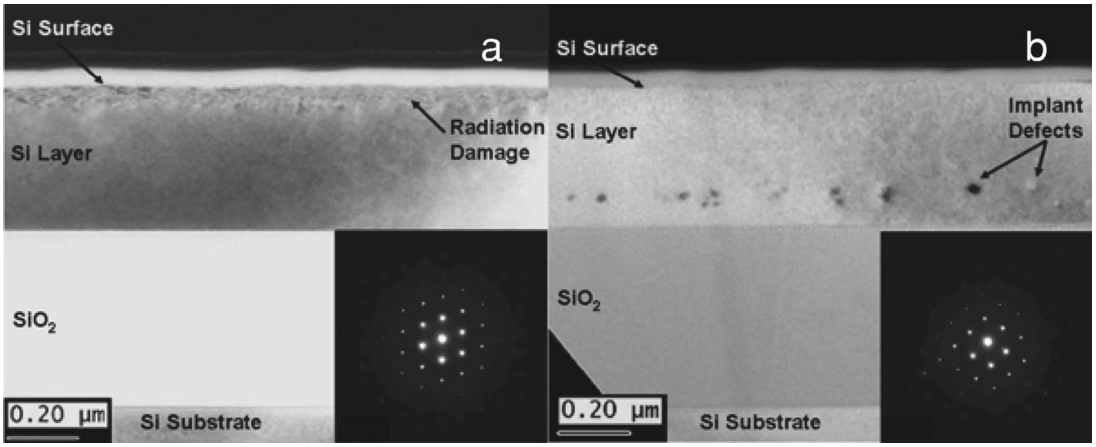

FIG. 4. Cross sectional transmission electron micrographs and selective area electron diffraction patterns of thin layers of silicon on insulator (a) "as cut" and (b) after several radiation repair anneals.

to repair any residual radiation damage incurred during the ion implantation of silicon, step (a) of Fig. 1. The XTEM image shown in Fig. 4(a) shows the presence of a small damage region near the surface of the transferred layer. Apart from this band of damage, the transferred layer is high quality single crystal silicon. The electron diffraction pattern shown in Fig. 4(a) is consistent with this result. The electron diffraction pattern is virtually indistinguishable from the electron diffraction pattern in Fig. 4(b), a sample with additional annealing up to 800 °C. This finding reinforces the observation made during RBS of the transferred layers in a [001] channeling orientation, Fig. 3 spectrum (c), that the microwave cut fabrication process keeps most the crystallinity of the silicon intact. This finding compares well with ion-cut processes involving conventional annealing to activate exfoliation of silicon.[21]

The damage shown in Fig. 4(a) is consistent with radiation damage from hydrogen and boron ions during the irradiation step of the microwave cut process, step (a) in Fig. 1.[8] Prior to any anneals, the majority of the radiation damage is present at the surface of the transferred layer, and the damage band encompasses approximately 25%, or 125 nm of the total layer thickness. TRIM[24] calculations for the implants of the sample in Fig. 4 yield straggle, or ΔR_p, values of approximately 100 nm for boron and 70 nm for hydrogen. For the given concentrations and energies of hydrogen and boron ions irradiating the sample, these results are consistent with previous papers.[9,20,22]

As can be seen in Fig. 4(b), after sequential anneals to repair radiation damage there is no visible damage near the surface of the transferred layer. The only visible damage appears near the bottom of the transferred layer. Note that in Figs. 4(a) and 4(b), the bottom of the transferred layer coincides with the top of the implanted material shown in Fig. 1, part (a). The damage seen in Fig. 4(b) can be accounted for as dislocation loops created during the sequential high temperature anneals of the sample. Intrinsic dislocation loops are created during postimplantation annealing, when shallow level vacancies which accompany deep level interstitials coagulate.[25] While vacancies by themselves usually anneal out of implanted silicon at temperatures around 550 °C, if dislocation loops form they can be stable up to 800 °C.[25] As with RBS, the cut depth of samples analyzed using XTEM ranged between 475 and 500 nm.

Figure 5 demonstrates the condition of the surface of a typical transferred layer in this work. The sample in Fig. 5 was fabricated using steps (a)–(d) in Fig. 1. The rms roughness of the sample as measured by AFM averaged 5.3 nm. There was little difference between the rms of blistered samples and that of samples including coherent layer transfer. Depending on implantation parameters, incubation times, and anneal temperatures, previously published microroughness values vary between 3.4 and 10 nm over 1 μm sampling distances.[20,21,26]

An established method of removing the lattice damage created during the ion-cut process is through a radiation repair treatment which consists of high temperature anneals.[9,20,26] Table I demonstrates the electrical behavior of as-cut and postannealed transferred layers fabricated using the ion-cut process shown in Fig. 1. Table I displays changes in resistivity, dominant carrier species, carrier concentration, and electronic mobility as a function of anneal temperature and time for successive high temperature anneals of a representative microwave-initiated exfoliated layer. Because previous research efforts used conventional annealing methods, the radiation repair anneals in this work were done using conventional means in order to attain higher temperatures

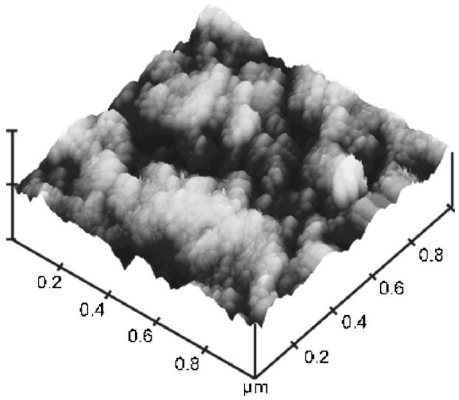

FIG. 5. Atomic force micrograph demonstrating the surface quality of thin layers of silicon on insulator in the "as-cut" state.

TABLE I. Hall effect electrical measurements obtained from a silicon donor substrate and a silicon-on-insulator transferred layer after microwave-initiated ion-cut exfoliation. The donor silicon was implanted with 9×10^{16} H^+ ions cm^{-2} at 50 keV and 2×10^{14} B^+ ions cm^{-2} at 175 keV.

Category	Description	Resistivity (Ω cm)	Type	Concentration	Mobility (cm^2/V s)
SOI	As exfoliated	3.83	*n*	5.49×10^{16} cm^{-3}	69
Donor Si	As exfoliated	3.88	*n*	1.3×10^{15} cm^{-2}[a]	57
SOI	500 °C, 2 h	4.2	*n*	6.2×10^{16} cm^{-3}	24
	600 °C, 2 h	4	*p*	2.13×10^{17} cm^{-3}	7
	700 °C, 2 h	0.0447	*p*	1.56×10^{18} cm^{-3}	89
	700 °C, 4 h	0.0374	*p*	2.05×10^{18} cm^{-3}	80
	800 °C, 2 h	0.0230	*p*	3.32×10^{18} cm^{-3}	82

[a]Sheet charge is reported because the damage layer thickness was not known exactly. The layer thickness can be estimated as $2R_p$, which would be approximately 1000 nm for this sample.

and to have a common reference point.[9,20,26] When viewing the data in Table I, most noteworthy is the change in conductivity type and the temperature of the anneals where this change takes place. Previous researchers have also observed this behavior, in which the surfaces of uncut samples start the fabrication process as *p* type, and after the cut step in Fig. 1(d) sample surfaces become *n* type. Upon successive anneals the transferred layer surfaces returned to *p* type.[9,20,26] Previous authors have proposed that the change in conductivity type upon exfoliation is due to the presence of hydrogen related shallow donors and hydrogen enhanced thermal donors.[3,9,20,27,28] Thermal donors can appear in hydrogen implanted materials when the implantation is followed by heating beyond 300 °C. Some of these thermal donors may be related to interstitial oxygen clusters in CZ grown silicon and become active in the presence of hydrogen at temperatures between 300 and 500 °C.[27,28] Although the implant temperatures used in this work did not approach 300 °C, the microwave exfoliation step of the ion-cut process [Fig. 1(d)] took place at temperatures 375–450 °C. At temperatures above 450 °C thermal donors begin to dissociate and at higher temperatures hydrogen diffuses out of silicon.[3,27,28] As a result, Table I demonstrates that *p*-type conductivity is regained after annealing the samples for 4 h at temperatures above 450 °C. Published values of *p*-type mobility in unetched samples range 9–121 cm^2/V s.[22,23,26]

In previous reports the carrier concentrations of samples measured after anneals above 650 °C were significantly lower ($\sim10^{16}$–10^{17} cm^{-3}) than the results attained here; unfortunately these papers did not have boron coimplants.[9,20,26] The authors believe that the change in hole carrier concentration is explained by electrical activation of some of the coimplanted boron. The hole mobilities attained in this work compare well with mobilities attained in single crystal silicon with the same carrier concentrations.[29]

DISCUSSION

Cut location in microwave enhanced ion-cut

A topic of interest in ion-cut fabrication is the ion-cut location and how that location correlates to known implant parameters. Knowledge of the implant parameters that determine the ion-cut location directly affects fabrication processes involving ion-cut samples. For this work there was interest in determining if a change in the ion-cut location occurs due to the use of microwaves during the anneal process. Although implanted ions in ion-cut processes become atoms as soon as they contact the implanted sample, several species within ion implanted silicon can react to the influence of a high frequency electric field. As a result, this work investigates the ion-cut location and how the location correlates with implant parameters when using microwave anneals, as opposed to conventional annealing.

How the cut location in ion-cut processes correlates with implant parameters has been the focus of debate since the inception of the ion-cut process. In the case of hydrogen only, or coimplanted boron and hydrogen species, Hochbauer *et al.* have asserted that the cut location correlates better with the peak in the TRIM[18] simulated hydrogen radiation damage profile and always coincides with the end-of-range damage, which depends on the concentration of implant species involved.[19,23] Lee *et al.* reported an effect in the ion-cut location due to the ion implant temperature, asserting that thicker layer transfer results when hydrogen ions are implanted at room temperature, as opposed to liquid helium temperatures.[20]

Table II summarizes pertinent implant parameters and ion-cut locations for the samples used in this work. As can be seen in Table II, three distinct exfoliation depths were seen in this work, and all sample sets except set E have exfoliation depths that do not coincide with the peak in the TRIM[18] simulated radiation damage or range profiles. The change in exfoliation depths as a function of implant species, dose, and temperature does agree with trends seen in previous ion-cut studies.[6–10,20,30]

Figure 6 presents a more detailed picture of the observed ion-cut locations for the transferred layers in this work and the complicated nature of how that location correlates to implant species, dose, and temperature. Figure 6(a) demonstrates the TRIM[18] simulated damage and concentration profiles for a sample similar to the implant parameters of sample set D in Table II, while Fig. 6(b) demonstrates damage and concentration profiles for a sample matching the implant parameters of sample set E in Table II. Also shown in the figure are the observed cut locations for processed samples.

As can be seen in Fig. 6(a) the implant damage induced by implanting 1×10^{15} B cm^{-2} into silicon is dwarfed by the

TABLE II. Experimentally measured ion-cut depths, experimental implant parameters, and TRIM simulated parameters for four sample sets used in microwave exfoliation.

Sample identifier	Implant temperature (K)	B^+ implant dose and energy	H^+ implant dose and energy	Hydrogen R_p (nm)[a]	Hydrogen D_p (nm)[a]	Cut depth (nm)
A	66	⋯	6×10^{16} cm^{-2} 40 keV	400	360	410
B	66	1×10^{15} cm^{-2} 147 keV	5×10^{16} cm^{2} 40 keV	400	360	410
C	300	⋯	1×10^{17} cm^{-2} 50 keV	475	440	500
D	300	2×10^{14} cm^{-2} 175 keV	9×10^{16} cm^{-2} 50 keV	475	440	500
E	300	3×10^{15} cm^{-2} 175 keV	9×10^{16} cm^{-2} 50 keV	475	440	475

[a]The hydrogen range and damage maxima were determined using TRIM computer code simulations.

damage created in implanting 9×10^{16} H cm^{-2}. Figure 6(a) demonstrates that in room temperature implants when the hydrogen-implant-induced damage exceeds the damage created by the boron implant, the exfoliation depth does not coincide with the peak in the hydrogen distribution. Höchbauer *et al.* have previously proposed that although implant-induced damage determines exfoliation depth, the exfoliation depths coincide with the end-of-range damage created during implantation rather than the peak in the implant damage because the peak in implant-induced damage also contains a large degree of fracture toughness.[19] In terms of Fig. 6(a), the end-of-range damage created during the hydrogen implant would lie to the right of the peak in the hydrogen damage distribution. This location also coincides with the vertical line denoting the observed exfoliation depth and seems to support the assertion of Höchbauer *et al.* In TRIM[18] simulated damage and range distributions for sample sets A and B in Table II (not shown) the exfoliation depth also occurred slightly deeper than the peak in radiation damage; but, because sample sets A and B were implanted at liquid nitrogen temperatures the exfoliation depths were closer to the peak in the implant damage than that shown in Fig. 6(a).

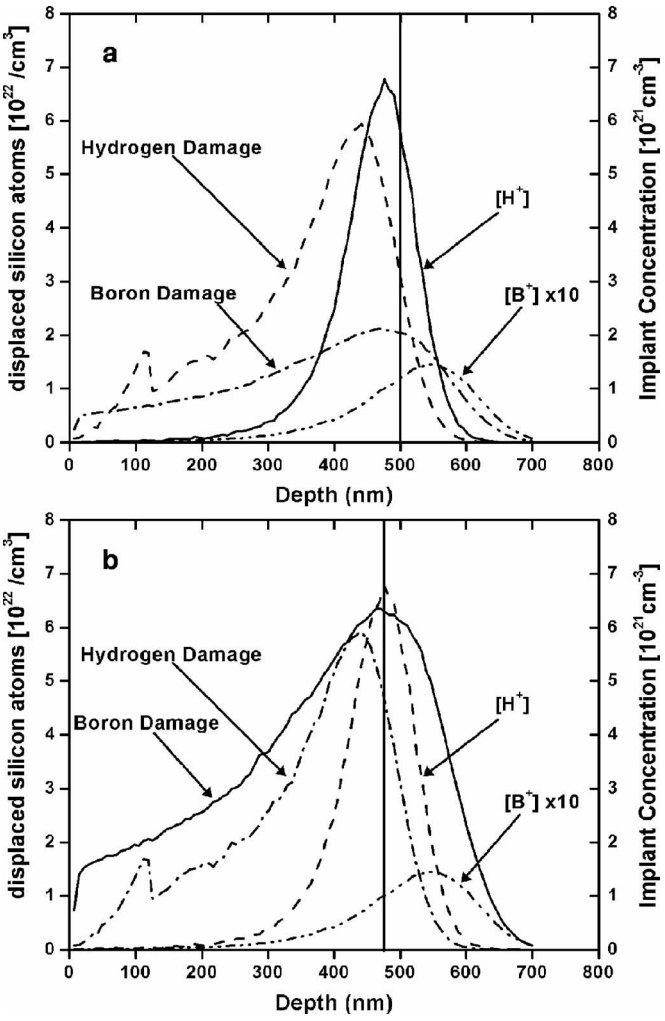

FIG. 6. TRIM (Ref. 24) simulated damage and range distributions in ion-implanted silicon showing (a) displaced silicon atoms for implants of 1×10^{15} B^+ cm^{-2} and 4.5×10^{16} H_2^+ cm^{-2} and (b) displaced silicon atoms for implants of 3×10^{15} B^+ cm^{-2} and 4.5×10^{16} H_2^+ cm^{-2}.

For samples implanted with boron at doses of 3×10^{15} cm^{-2} Fig. 6(b) shows that the boron-implant-induced damage profile is higher than that for the hydrogen implant. In these samples, the ion-cut location shifted to a shallower location as compared to samples implanted with lower doses of boron. The shift in the ion-cut depth cannot be explained by implant temperature as sample sets D and E were both implanted at room temperature.

The change in the cut location between Figs. 6(a) and 6(b) appears to be solely due to the boron concentration differences. Previous research has shown that boron coimplants reduce the as-implanted radiation damage within the implanted sample[10,31] and that high boron concentrations promote self-diffusion and recrystallization rates in silicon.[32] As a result, high concentrations of boron promote fast recovery of the implant-induced damage in ion implanted samples. This fast recovery takes place throughout the damage region, and if the boron implant concentration is high enough, can lead to a shift in the peak of the radiation damage profile compared to hydrogen only implants.[10,32] Equation (1) demonstrates the effect of the implant dose Q_I and the concentration profile straggle ΔR_p on the as-implanted peak implant species concentration N_m:

$$N_m = \frac{Q_1}{\sqrt{2\pi\Delta R_p^2}}. \quad (1)$$

The calculated peak boron concentration for sample set D in Table II is approximately 8×10^{18} cm^{-2}. That of sample set E in Table II is approximately 1.2×10^{20} cm^{-2}. Therefore, the samples implanted with the highest concentration of boron had a significant shift in the implantation damage due to fast recovery, whereas the samples implanted with lower concentrations of boron did not. Although sample set B in Table II also has a high concentration of implanted boron, sample set B was implanted at liquid nitrogen temperatures, thus inhibiting self-diffusion and fast recovery.

The ion-cut locations realized in this work are in good agreement with the work from previous authors using a vacuum or mechanical furnace. As a result, we infer that microwave initiation of the exfoliation process has not resulted in any significant physical effects that might lead to changing of the ion-cut exfoliation location.

Microwave heating of ion-cut materials

In contrast to traditional convective, conductive, and radiative heating, in which a sample surface is heated, microwave heating is characterized as being volumetric in nature. Microwaves penetrate into a sample and effectively heat a near surface volume simultaneously. How much microwave power is absorbed and how deep the absorbance occurs determine how effective microwaves are in heating a material. Heating in a semiconductor material takes place as microwave power is absorbed and transferred to heat through microwave loss mechanisms.[17] The mechanisms of interest in microwave heating of ion-cut fabricated samples are conduction and polarization.

Microwave conduction losses occur as a consequence of electron drift, where free electrons in the extrinsic silicon move in response to an applied electric field. Conduction effects are commonly referred to as Ohmic effects. Microwave polarization losses occur in extrinsic silicon due to electric polarization, dipolar polarization (also referred to as dipolar reorientation and dielectric relaxation), and Maxwell-Wagner or interfacial polarization. Electric polarization occurs when electrons are displaced from their equilibrium positions around nuclei in response to an applied electric field. Dipolar polarization occurs in extrinsic silicon as a consequence of coupled defects such as vacancy-vacancy or vacancy-interstitial pairs interacting with applied electric fields.[33] Maxwell-Wagner polarizations can manifest as an accumulation of charge at the interface between two heterogeneous dielectric media such as silicon and silicon dioxide, or extrinsic silicon and a highly resistive layer formed by ion implantation.[17]

An important materials parameter that captures the effect of conduction and polarization loss mechanisms in microwave heating of extrinsic silicon is the loss factor ε''. The loss factor can be thought of as a materials parameter that describes the difference between a real dielectric, in which losses occur, and an ideal dielectric.

Traditionally, the complex permittivity includes the effect of conduction losses through the inclusion of the loss factor; but, the loss factor can be augmented to include the effect of polarization as well.[17,33,34] When the loss factor includes the effects of both conduction and polarization it is called an effective loss factor. The effective loss factor representing all loss mechanisms in extrinsic silicon is shown as follows:

$$\varepsilon''_{\text{eff}}(\omega)=\varepsilon''_{e}(\omega)+\varepsilon''_{d}(\omega)+\varepsilon''_{\text{MW}}(\omega)+\varepsilon''_{c}(\omega), \tag{2}$$

where ω represents the angular frequency of the microwaves, and the subscripts e, d, MW, and c correspond to the effective loss factor contributions from electric polarization, dipolar polarization, Maxwell-Wagner polarization, and conduction. Both the power absorbed by extrinsic silicon and the penetration depth depend on the effective loss factor as follows:

$$P_{\text{abs}}=\omega\varepsilon_0\varepsilon''_{\text{eff}}|E|^2, \tag{3}$$

$$D_p=\frac{\lambda_0}{2\pi(2\varepsilon')^{1/2}}\{[1+(\varepsilon''_{\text{eff}}/\varepsilon')^2]^{1/2}-1\}^{-1/2}. \tag{4}$$

In Eq. (3) P_{abs} is on a per volume basis, ε_0 represents the permittivity of free space, and E is the root mean square internal electric field. In Eq. (4) λ_0 is the wavelength of the penetrating microwaves, $\varepsilon''_{\text{eff}}$ is the effective loss factor, and ε' is the real component of the complex permittivity. D_p is the approximate depth to which e^{-1} or 36.8% of the impinging microwave electric field penetrates the surface.

Previous researchers have approximated microwave penetration into silicon using a characteristic skin depth calculated assuming only Ohmic losses in silicon:[35]

$$\delta_s=\sqrt{\frac{\rho}{\pi(f)\mu_0}}, \tag{5}$$

where δ_s is the characteristic skin depth, ρ signifies the silicon resistivity in Ω cm, (f) the frequency of the microwaves, and μ_0 the permeability of free space $(4\pi\times10^{-9}$ H cm$^{-1})$. Although Eq. (5) does not account for polarization losses, it uses readily available data and can approximate D_p in Eq. (4). Using Eq. (5) as an approximation, the characteristic skin depth at which 63% the incident microwave power penetrates into the silicon samples used for this work ranged 0.03–0.3 cm. The wafers used to fabricate the ion-cut samples in this work ranged in thickness from 0.04 to 0.05 cm and as one can see by viewing Fig. 1(c) the ion-cut region of interest, where the exfoliation takes place, corresponds to $(0.04\pm5)\times10^{-7}$–$(0.05\pm5)\times10^{-7}$ cm deep from the surface of the bonded samples. Because at least 63% of the incident microwaves reach the ion-cut region of interest we assert that during microwave heating the ion-cut region is heated by microwave heating alone, i.e., no conduction or convection.

The power absorbed in microwaved materials is converted to heat within the materials according to Eq. (6).[36] In Eq. (6), P represents the net absorbed power, m the mass of silicon, C_p the specific heat of silicon, T the temperature of silicon, and t the time.

$$P=mC_p\frac{\Delta T}{dt}. \tag{6}$$

Microwave enhancement in ion-cut fabrication

The ion-cut samples that were microwave processed for this work saw a decrease in the required exfoliation times in comparison with previously published values. Although the times to exfoliate were reduced, the temperatures of the samples at the time of the exfoliation were between 375 and 450 °C depending on process time, similar to other ion-cut processes. This decrease in exfoliation time can be attributed, in part, to the volumetric heating and penetration depth associated with microwave heating of extrinsic silicon. Equations (3) and (5) demonstrate that at any heating time greater than time zero, the alternating electric field magnitude is constant at the ion-cut region.

An important factor that may contribute to the reduced exfoliation times of microwave-heated ion-cut samples is an increase in the flux of vacancy point defects due to the electric fields present. Vacancies have been proposed as a mechanism by which hydrogen platelets nucleate and grow in ion-cut processing.[37,38] In extrinsic silicon, vacancies have an associated charge state.[5] Charged species can be influenced by electric fields. Work by Freeman *et al.* demonstrated increased ionic currents in salt crystals during microwave radiation due exclusively to the presence of microwave fields. Freeman *et al.* attributed the increased ionic currents to an increase in charged vacancy flux when under the influence of microwave radiation.[39] Similarly, charged vacancies should be affected by microwave fields in silicon. In this way, the electric fields created by microwave heating may serve to enhance vacancy migration by increasing the net flux of vacancies to the nearest sink, the nucleated hydrogen platelets.

CONCLUSION

Microwave heating has been employed as an alternative to conventional heating in the exfoliation of silicon and the ion-cut process. RBS, XSEM, XTEM, selected area electron diffraction (SAED), Hall effect, and TRIM simulation have shown that little physical difference exists between the end product of microwave enhanced exfoliation and exfoliation through conventional heating. For boron implant doses of 2×10^{14}–3×10^{15} cm^{-2} the cut location correlates well with the hydrogen-implant-induced end-of-range damage.

Samples processed for this work saw a slight decrease in exfoliation times. Equations are presented which explain microwave absorption by extrinsic silicon. Skin depth calculations demonstrate that microwave power penetrates silicon down to the ion-cut region of interest. We believe that the mechanism responsible for the decrease in exfoliation time may include enhanced vacancy fluxes due to the presence of electric fields. As a result, the implant-induced damage that arises in silicon during ion-cut fabrication serves to decrease processing times. This is a significant and beneficial side effect of creating radiation damage in ion-cut samples.

ACKNOWLEDGMENTS

The authors would like to acknowledge the Structure/Property Relations Group, Materials Science and Technology Division, Los Alamos National Labs for their assistance with ion implantation. This work was partially supported by a grant from the NSF (DMR-0308127, L. Hess) and a Strategic Research Grant from City University of Hong Kong (SRG No. 7001820). The work at Los Alamos National Laboratory was supported by the DOE Office of Basic Energy Sciences.

[1] M. Bruel, Electron. Lett. **31**, 1201 (1995).
[2] M. Bruel, Nucl. Instrum. Methods Phys. Res. B **108**, 131 (1996).
[3] J. Pearton, W. Corbett, and M. Stavola, *Hydrogen in Crystalline Semiconductors*, Springer Series in Materials Science Vol. 16 (Springer, New York, 1992).
[4] C. Maleville and C. Mazure, Solid-State Electron. **48**, 1055 (2004).
[5] J. W. Mayer and S. S. Lau, *Electronic Material Science: For Integrated Circuits in Si and GaAs* (Macmillan, New York, 1990).
[6] T. Höchbauer and M. Nastasi, Appl. Phys. Lett. **75**, 3938 (1999).
[7] T. Höchbauer, A. Misra, R. Verda, and M. Nastasi, Philos. Mag. B **80**, 1921 (2000).
[8] T. Höchbauer, A. Misra, and M. Nastasi, J. Appl. Phys. **89**, 5980 (2001).
[9] M. Cai *et al.*, J. Appl. Phys. **92**, 3388 (2002).
[10] T. Höchbauer, K. C. Walter, R. B. Schwarz, M. Nastasi, R. W. Bower, and W. Ensinger, J. Appl. Phys. **86**, 4176 (1999).
[11] L. Shao *et al.*, Appl. Phys. Lett. **87**, 091902 (2005).
[12] R. Subasri, T. Matthews, O. M. Sreedharan, and V. S. Ragunathan, Solid State Ionics **158**, 199 (2003).
[13] R. Roy, D. Agrawal, J. Cheng, and S. Gedevanishvili, Nature (London) **399**, 668 (1999).
[14] S. Aravindan, J. Ramkumar, and R. Krishnamurthy, Ceram. Trans. **111**, 287 (2001).
[15] D. C. Thompson, H. C. Kim, T. L. Alford, and J. W. Mayer, Appl. Phys. Lett. **83**, 3918 (2003).
[16] D. C. Thompson *et al.*, Appl. Phys. Lett. **87**, 224103 (2005).
[17] A. C. Metaxas and R. J. Meredith, *Industrial Microwave Heating*, IEEE Power Engineering Series 4 (Peter Peregrinus Ltd., London, UK, 1983).
[18] L. R. Doolittle, Nucl. Instrum. Methods Phys. Res. B **B9**, 344 (1985).
[19] T. Höchbauer, A. Misra, M. Nastasi, K. Henttinen, T. Suni, I. Suni, S. S. Lau, and W. Ensinger, Nucl. Instrum. Methods Phys. Res. B **216**, 257 (2004).
[20] J. K. Lee, M. Nastasi, N. D. Theodore, A. Smalley, T. L. Alford, J. W. Mayer, M. Cai, and S. S. Lau, J. Appl. Phys. **96**, 280 (2004).
[21] J. Du, W. H. Ko, and D. J. Young, Sens. Actuators, A **112**, 116 (2004).
[22] V. P. Popov *et al.*, Mater. Sci. Eng., B **73**, 82 (2000).
[23] T. Höchbauer, A. Misra, M. Nastasi, and J. W. Mayer, J. Appl. Phys. **92**, 2335 (2002).
[24] J. F. Zeigler, IBM Research, Yorktown, NY 10598.
[25] K. S. Jones, S. Prussin, and E. R. Weber, Appl. Phys. A: Solids Surf. **45**, 1 (1988).
[26] F. Lu *et al.*, J. Vac. Sci. Technol. B **21**, 2109 (2003).
[27] H. J. Stein and S. K. Hahn, J. Appl. Phys. **75**, 3477 (1994).
[28] H. J. Stein and S. K. Hahn, Appl. Phys. Lett. **56**, 63 (1990).
[29] R. F. Pierret, *Semiconductor Device Fundamentals* (Addison-Wesley, Reading, MA, 1996).
[30] M. Nastasi, T. Höchbauer, J.-K. Lee, A. Misra, and J. P. Hirth, Appl. Phys. Lett. **86**, 154102 (2005).
[31] J. K. Lee, T. Höchbauer, R. D. Averitt, and M. Nastasi, Appl. Phys. Lett. **83**, 3042 (2003).
[32] K. Henttinen, T. Suni, A. Nurmela, I. Suni, S. S. Lau, T. Höchbauer, M. Nastasi, and V.-M. Airaksinen, Nucl. Instrum. Methods Phys. Res. B **190**, 761 (2002).
[33] B. Meng, B. D. B. Klein, J. H. Booske, and R. F. Cooper, Phys. Rev. B **53**, 12777 (1996).
[34] J. H. Booske, R. F. Cooper, S. A. Freeman, K. I. Rybakov, and V. E. Semenov, Phys. Plasmas **5**, 1664 (1998).
[35] S.-L. Zhang, R. Buchta, and D. Sigurd, Thin Solid Films **246**, 151 (1994).
[36] D. R. Gaskell, *Introduction to the Thermodynamics of Materials* (Taylor & Francis, Levittown, PA, 1995).
[37] M. K. Weldon *et al.*, J. Vac. Sci. Technol. B **15**, 1065 (1997).
[38] M. Nastasi, T. Höchbauer, J.-K. Lee, A. Misra, and J. P. Hirth, Appl. Phys. Lett. **86**, 154102 (2005).
[39] S. A. Freeman, J. H. Booske, and R. F. Cooper, Phys. Rev. Lett. **74**, 2042 (1995).